F-actin prevents interaction between sperm DNA and the oocyte meiotic spindle in *C. elegans*

Michelle T. Panzica,[1] Harold C. Marin,[1] Anne-Cecile Reymann,[2] and Francis J. McNally[1]

[1]Department of Molecular and Cellular Biology, University of California, Davis, Davis, CA
[2]BIOTEC TU Dresden, Dresden, Germany

Fertilization occurs during female meiosis in most animals, which raises the question of what prevents the sperm DNA from interacting with the meiotic spindle. In this study, we find that *Caenorhabditis elegans* sperm DNA stays in a fixed position at the opposite end of the embryo from the meiotic spindle while yolk granules are transported throughout the embryo by kinesin-1. In the absence of F-actin, the sperm DNA, centrioles, and organelles were transported as a unit with the yolk granules, resulting in sperm DNA within 2 µm of the meiotic spindle. F-actin imaging revealed a cytoplasmic meshwork that might restrict transport in a size-dependent manner. However, increasing yolk granule size did not slow their velocity, and the F-actin moved with the yolk granules. Instead, sperm contents connect to the cortical F-actin to prevent interaction with the meiotic spindle.

Introduction

Fertilization occurs during female meiosis in most animals, resulting in the presence of paternal chromosomes and centrioles in the same cytoplasm with the oocyte meiotic spindle for periods ranging from 45 min in *Caenorhabditis elegans* (Yang et al., 2003) to 2 h in mice (Deguchi et al., 2000). Sperm-derived centrioles mature by recruiting maternal pericentriolar proteins to nucleate microtubule asters that capture the female pronucleus after completion of meiosis. Therefore, animals must prevent sperm asters from interfering with meiotic spindles until after extrusion of the second polar body. Several species suppress sperm aster formation until the completion of meiosis (Gould and Stephano, 1999; Stephano and Gould, 2000; McNally et al., 2012). The significance of this suppression was illustrated in *C. elegans* by RNAi depletion of the kinesin-binding protein KCA-1, which results in premature centrosome maturation and sperm aster formation. In cases where the premature sperm aster came within 16 µm of the meiosis II spindle, the spindle was captured by the sperm aster, preventing extrusion of the second polar body and thus generating a triploid embryo (McNally et al., 2012). The low frequency (6/24) of the sperm approaching the meiotic spindle within the threshold distance suggests that an active mechanism of sperm positioning exists during *C. elegans* female meiosis.

In *C. elegans*, the physical separation of sperm from the meiotic spindle originates with a kinesin-dependent migration of the germinal vesicle away from the future sperm entry site (Goldstein and Hird, 1996; McCarter et al., 1999; McNally et al., 2010). Then, the meiotic spindle assembles at the opposite end of the oocyte from the sperm entry point. In mice, fertilization also occurs away from the spindle, as the spindle generates a microvilli-free zone on the overlying cortex (Verlhac et al., 2000), and microvilli are required for sperm–egg fusion (Runge et al., 2007). After fertilization, early *C. elegans* meiotic embryos exhibit cytoplasmic streaming in which kinesin-1 transports yolk granules inward from the cortex and around the entire embryo (McNally et al., 2010). Loss of kinesin-1 results in sperm closer to the cortex, suggesting that kinesin-1 initially transports the sperm inward after fertilization (McNally et al., 2012). Cytoplasmic streaming toward the meiotic spindle also occurs in mice (Yi et al., 2011). Thus, some mechanism must exist for the sperm to resist cytoplasmic streaming and maintain a distance from the meiotic spindle. This mechanism has not been previously addressed in any species. Here, we report an F-actin–dependent mechanism that maintains the separation of the sperm DNA and organelles from the female meiotic spindle during meiotic cytoplasmic streaming in *C. elegans*.

Results and discussion

Proper sperm DNA positioning requires profilin, F-actin, and formins

To test whether F-actin is required for sperm DNA positioning, embryos were depleted of F-actin by either profilin RNAi or latrunculin A treatment. To ensure that F-actin was depleted, we only scored *pfn-1(RNAi)* or latrunculin-treated embryos with clear signs of polar body failure (see the RNA interference and drug treatments section of Materials and methods). Control embryos restricted the sperm DNA within 60–90% embryo length from the spindle (Fig. 1, A and B). *pfn-1(RNAi)* (*n* =

Correspondence to Francis J. McNally: fjmcnally@ucdavis.edu

Abbreviation used: MSD, mean-squared displacement.

The Rockefeller University Press
J. Cell Biol. Vol. 216 No. 8 2273–2282
https://doi.org/10.1083/jcb.201702020

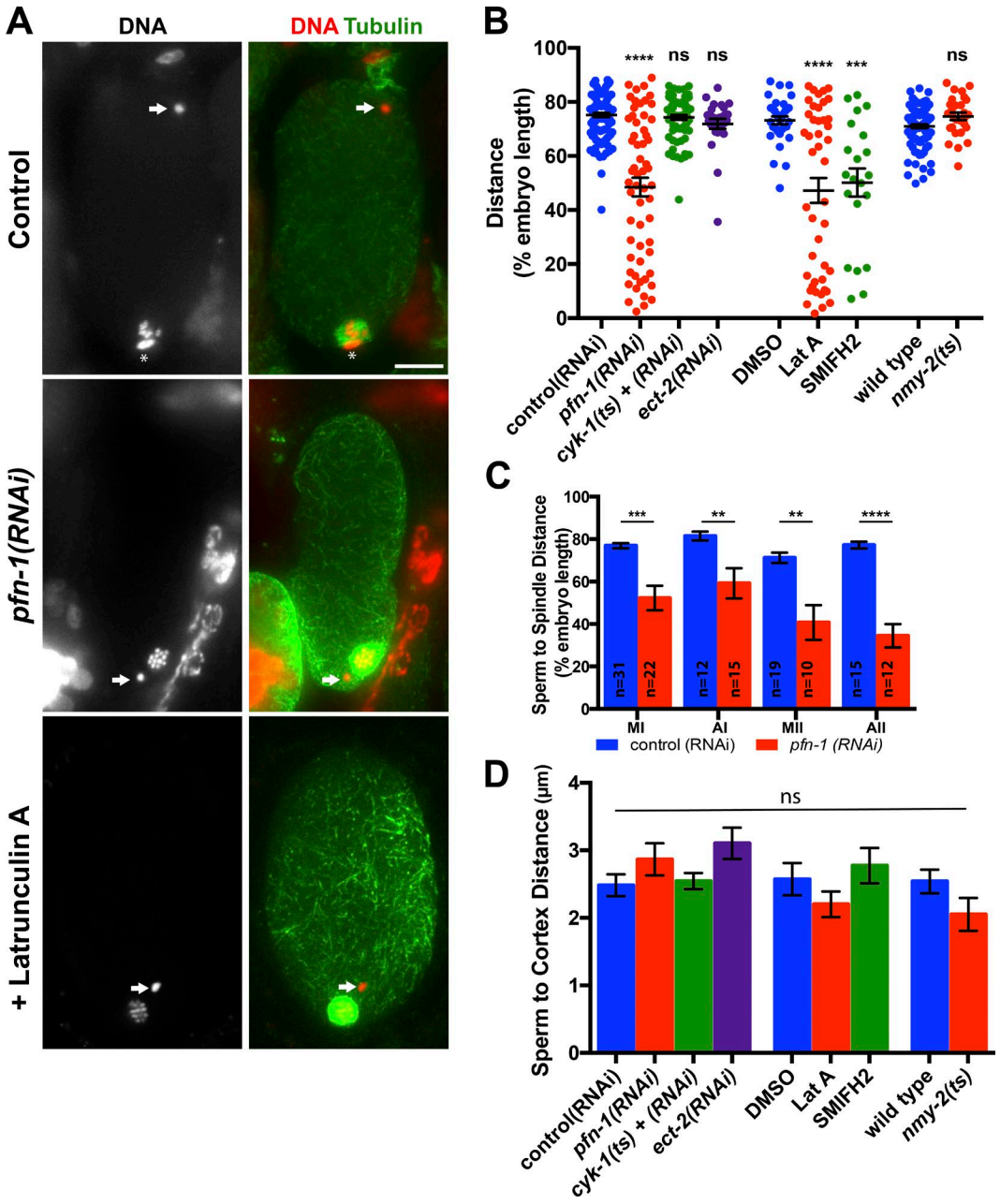

Figure 1. **F-actin is required for sperm DNA positioning.** (A) Maximum intensity projections of control(RNAi)-, *pfn-1(RNAi)*–, or latrunculin A–treated fixed meiotic embryos. Asterisks indicate a polar body; arrows indicate sperm DNA location. Bar, 10 µm. (B) Sperm-to-spindle distance for meiotic embryos at all stages. Lat A, latrunculin A. Numbers are listed in Table S1. (C) Sperm-to-spindle distance for control and *pfn-1(RNAi)* meiotic embryos by stage. AI, anaphase I; AII, anaphase II, MI, metaphase I; MII, metaphase II. (D) Sperm-to–nearest cortex distance for embryos at all stages of meiosis. Numbers are listed in Table S1. **, P < 0.01; ***, P < 0.001; ****, P < 0.0001; two-tailed *t* test. Error bars denote standard error of the mean.

59) or latrunculin A ($n = 44$) resulted in sperm DNA positioned throughout the embryo (0–90% embryo length from the spindle; Fig. 1, A and B; and Table S1). Sperm DNA positioning defects were observed at all stages of meiosis (Fig. 1 C). Interestingly, the distance between the sperm DNA and the closest cortex remained unchanged upon *pfn-1(RNAi)* or latrunculin A treatment (Fig. 1 D and Table S1). These results suggest that profilin and F-actin are required to accurately position the sperm DNA away from the spindle but not necessarily the cortex.

Profilin binds to formins (Chang et al., 1997; Evangelista et al., 1997; Watanabe et al., 1997) and is required for formins to efficiently assemble F-actin (Sagot et al., 2002). Thus, we initially tested the requirement of the well-characterized formin CYK-1, which is required for embryonic cytokinesis (Swan et al., 1998) and directly binds PFN-1 (Severson et al., 2002), but found no effect on sperm position (Fig. 1, B and D; and Table S1). The small molecule SMIFH2 (Rizvi et al., 2009) was used to test the requirement of all nine *C. elegans* formins (Mi-Mi et al., 2012) in sperm positioning. Similar defects in sperm-to-spindle distance were observed in SMIFH2-treated embryos ($n = 21$) as in *pfn-1(RNAi)*– or latrunculin A–treated embryos (Fig. 1 B and Table S1). Additionally, the distance between the sperm and the cortex remained unchanged in SMIFH2-treated embryos (Fig. 1 D and Table S1). Together, these results suggest

that formins other than CYK-1 are required for proper sperm positioning away from the spindle.

Formins are regulated by the Rho family of GTPases, and during polarization and cytokinesis of the *C. elegans* zygote, attention has been focused on RHO-1 and the Rho guanine nucleotide exchange factor (RhoGEF) ECT-2 (Motegi and Sugimoto, 2006a,b). However, depleting ECT-2 via RNAi to a level that blocked polar body formation had no effect on sperm position (n = 26; Fig. 1, B and D; and Table S1). This could be because of an incomplete knockdown of ECT-2 or could indicate that the formins responsible for positioning the sperm contents are regulated by different GEFs and Rho family GTPases as occurs in tubulogenesis (Shaye and Greenwald, 2016). Next, to test the requirement of myosin contractility for sperm positioning, we used a fast-acting temperature-sensitive allele of the nonmuscle myosin NMY-2 that is required for polar body formation. Analysis of meiotic embryos with failed polar body formation produced by *nmy-2(ts)* mutants grown at nonpermissive temperature did not result in sperm positioning defects (Fig. 1, B and D; and Table S1). This result could indicate that myosin II was not completely inactivated or that contractile myosin II is not required for sperm positioning.

Profilin and F-actin restrict sperm DNA movement

With the large variation of sperm DNA positions found in fixed *pfn-1(RNAi)* embryos, we sought to distinguish whether this resulted from a change in fertilization site or sperm DNA movement after fertilization. Using time-lapse microscopy of embryos expressing mCherry::histone, GFP::tubulin, and GFP::vitellogenin (yolk), sperm DNA was tracked during metaphase I in control(RNAi) and *pfn-1(RNAi)* (Fig. 2, A–C; and Videos 1–3). In controls (n = 10), sperm DNA remained restricted to a small area on the opposite side of the embryo from the meiotic spindle (Fig. 2, A–C; and Video 1). In contrast, sperm DNA in *pfn-1(RNAi)* embryos (n = 10) was initially positioned correctly and then moved over large distances similar to the yolk granules (Fig. 2, A–C; Video 2). The maximum displacement of sperm DNA during a 30-s interval increased upon *pfn-1(RNAi)* treatment (Fig. 2 D). In addition, both the peak and average velocity of sperm DNA movement was significantly higher in *pfn-1(RNAi)* (Fig. 2 E). Consistent with data obtained from fixed embryos, sperm DNA stayed close to the cortex during movement in *pfn-1(RNAi)* (Video 3; in Fig. 2 B and Video 2, the sperm DNA is moving along the cortex closest to the objective). Analysis by mean-squared displacement (MSD) of all trajectories combined revealed that sperm DNA normally undergoes movement consistent with free diffusion (α = 1.06) but, in the absence of profilin, is more similar to active transport or super diffusion (α = 1.53; Fig. 2, F–H). Together, these results eliminate altered sperm entry site as the cause for the variation in sperm DNA position. Rather, in the absence of profilin, the sperm DNA enters at a normal position away from the meiotic spindle and subsequently moves throughout the embryo. These results indicate that F-actin restricts movement of sperm DNA within the zygote.

Sperm DNA movement is dependent on kinesin-1

We hypothesized that sperm DNA movement in *pfn-1(RNAi)* would depend on the *C. elegans* kinesin-1 UNC-116 because sperm DNA and yolk granules appeared to move in the same direction and at the same velocity (McNally et al., 2012), similar to the UNC-116–dependent movements of cortical granules and the endoplasmic reticulum (Kimura et al., 2017). We used the *unc-116(f130)* ts allele, as UNC-116 still localizes around the sperm DNA but prevents premature centrosome maturation (McNally et al., 2012). Because spindle position is variable in *unc-116(f130)*, we measured the absolute position for both the sperm and spindle, where the embryo edge closest to the sperm was designated 0% (Fig. 3, A and B). In control embryos grown at 25°C (the nonpermissive temperature for *unc-116[f130]*), the absolute position of the sperm ranged from 1.6 to 17.6% embryo length (n = 31). In *pfn-1(RNAi)* embryos grown at 25°C, the absolute position of the sperm DNA ranged from 3.6 to 43.9% embryo length (n = 19), where the absolute position cannot exceed 50% by this quantification (Fig. 3 C). However, the broad distribution of sperm DNA positions seen in *pfn-1(RNAi)* was reduced to 2.2–18.3% embryo length in *pfn-1(RNAi);unc-116(f130)* embryos grown at 25°C (n = 36), which is not significantly different from control or *unc-116(f130)* embryos grown at 25°C (Fig. 3 C). This suggests that sperm DNA is transported in a kinesin-1–dependent manner in *pfn-1(RNAi)* embryos. Consistent with previous studies, *unc-116(f130)* embryos grown at 25°C exhibited a significant reduction in the sperm DNA–to-cortex distance compared with control embryos (Fig. 3 D and Table S1; McNally et al., 2012).

Both myosin V and dynein have been shown to bind and slow kinesin-1 cargos (Serbus et al., 2005; Kapitein et al., 2013). If myosin V or dynein function to restrict kinesin-1 movement, we would expect to see an increase in sperm-to-cortex distance upon their depletion. Analysis of sperm DNA position in fixed meiotic embryos from *hum-2(ok596)* (a presumptive null allele of myosin V; Baker and Titus, 1997) worms revealed no defects in sperm-to-cortex distance (Fig. 3 D). Distance between the sperm DNA and the closest cortex also remained unchanged upon depletion of dynein to an extent that allowed ovulation but blocked centrosome separation in the first mitosis (Fig. 3 D and Table S1; Yoder and Han, 2001). Under the conditions tested, neither myosin V nor dynein were required to oppose inward transport of the sperm DNA by kinesin-1. It remains possible that more complete depletions or double depletions of myosin V or dynein with F-actin might alter the transport of sperm DNA.

The sperm contents move as a cohesive unit after fertilization

Our results indicated that the wild-type F-actin cytoskeleton allows kinesin-dependent transport of yolk granules but not the transport of the sperm DNA. In starfish oocytes, a contracting F-actin meshwork moves large cargo faster than small cargo, indicating that a cytoplasmic actin meshwork can act as a size-dependent sieve (Mori et al., 2011). We hypothesized that a stationary, rather than contractile, F-actin meshwork acts as a sieve to restrict transport of large kinesin cargo. An alternative hypothesis is that some component of the sperm is tethered to the cortical F-actin. For either model, it is essential to know the effective size of the sperm contents within the meiotic embryo. In addition to DNA, *C. elegans* sperm also contain two centrioles, mitochondria, membranous organelles, and proteasomes (Ward et al., 1981; Pelletier et al., 2004; Al Rawi et al., 2011; Hajjar et al., 2014). We stained embryos for the centrosomal protein SPD-2 to investigate whether the centrioles stay linked with the sperm DNA in *pfn-1(RNAi)*. In control embryos, we observed SPD-2 in a ring around the sperm DNA

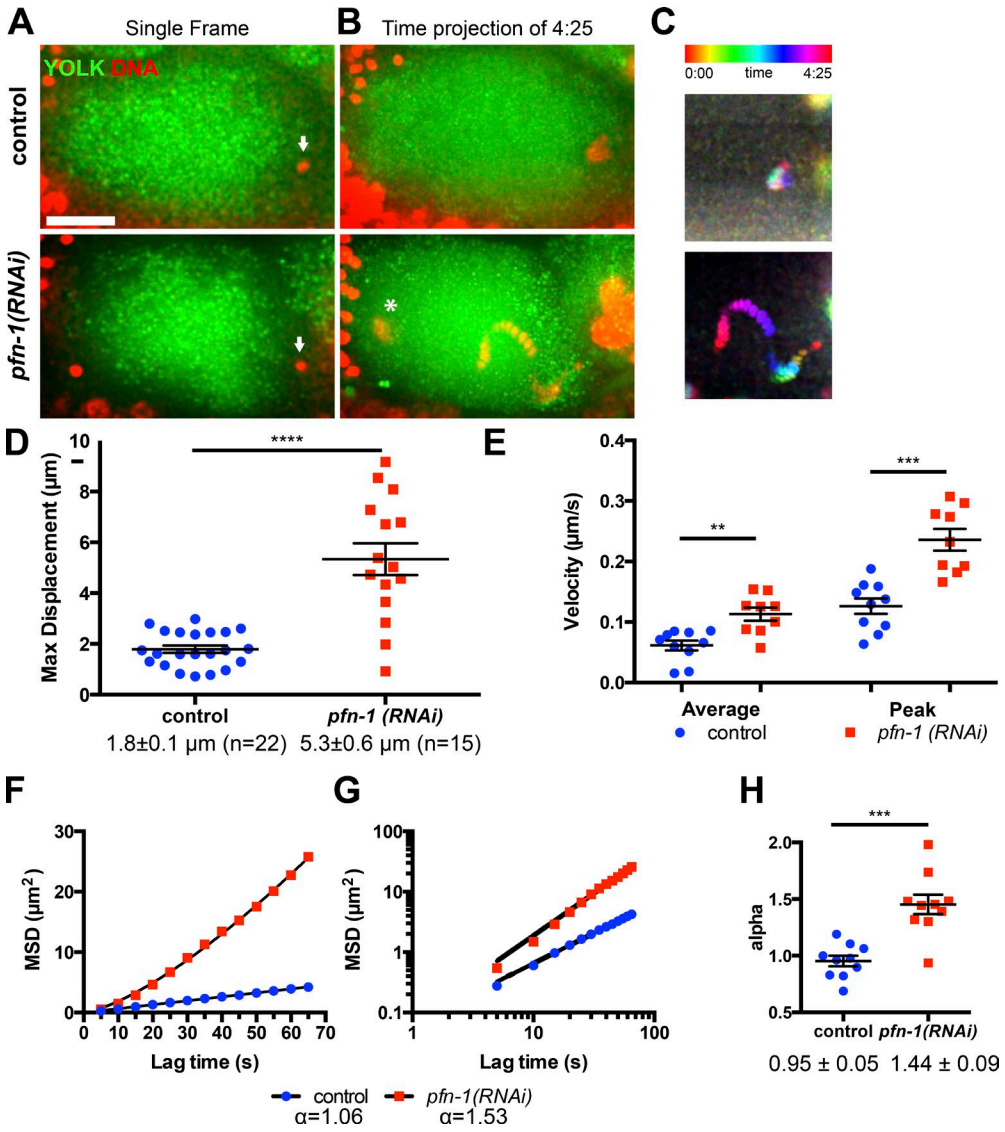

Figure 2. **Sperm DNA is actively transported in *pfn-1(RNAi)*.** (A–C) Single frame (A) and time projection (B) from a time-lapse image of a control and *pfn-1(RNAi)* meiotic embryo expressing GFP::yolk and mCherry::histone. The asterisk marks the spindle DNA that was present for a few frames. Arrows point to sperm DNA. Bar, 10 µm. (C) Temporal color code to indicate sperm position through time. The scale is the same as in A and B. (D) Maximum (Max) 2D displacement of sperm DNA over a 30-s period. (E) Average and peak velocity of sperm DNA movement acquired at 5-s intervals. Average velocity: control = 0.06 ± 0.01 µm/s (n = 10); *pfn-1(RNAi)* = 0.11 ± 0.01 µm/s (n = 10). Peak velocity: control = 0.13 ± 0.01 µm/s (n = 10); *pfn-1(RNAi)* = 0.23 ± 0.02 µm/s (n = 10). (F and G) Average 3D MSD calculated from trajectories of sperm DNA plotted with linear (F) and logarithmic (G) axes. Images were acquired at a 5-s interval. Alpha for control = 1.06 (n = 10); alpha for *pfn-1(RNAi)* = 1.53 (n = 10). (H) Scatter plot of individual alphas from MSD plots of each time-lapse image captured used for analysis in F and G. n = 10. **, P < 0.01; ***, P < 0.001; ****, P < 0.0001; two-tailed t test. Error bars denote standard error of the mean.

with bright foci marking the centrioles (n = 29; Fig. 4 A). In 11/11 *pfn-1(RNAi)* embryos with mispositioned sperm DNA, the SPD-2 staining pattern was indistinguishable from controls (Fig. 4 B), showing that the centrioles stay associated with the sperm DNA during movement.

After fertilization, maternal GFP::ubiquitin colocalizes with the sperm proteasomes and membranous organelles (Al Rawi et al., 2011; Hajjar et al., 2014). Using ubiquitin as a marker for sperm organelles, we tested whether these organelles stay associated with the sperm DNA upon profilin depletion in live embryos. In 14/14 control embryos, the organelles surrounded the sperm DNA (Fig. 4 C). In 10/10 *pfn-1(RNAi)* embryos with sperm position defects, the organelles maintained their position around the sperm DNA (Fig. 4 C). During time-lapse imaging of one *pfn-1(RNAi)* embryo, the sperm organelles and DNA moved throughout the embryo (Fig. 4 D). Together these observations revealed that the sperm contents stay together as a unit after fertilization within the oocyte and move together upon *pfn-1(RNAi)*, despite the absence of a surrounding membrane after fertilization (Takayama and Onami, 2016).

The finding that the sperm contents moved as a cohesive unit indicated that the sperm DNA, centrioles, and organelles are somehow bound together. Therefore, we reevaluated the distance of the sperm from the cortex and the size of the sperm contents in the zygote. Measurement of sperm organelles to the closest cortex in metaphase I revealed that the sperm-to-cortex distance was only 1.1 ± 0.1 µm (n = 14; Fig. 4 E), significantly less than the distance between the sperm DNA and cortex (2.6

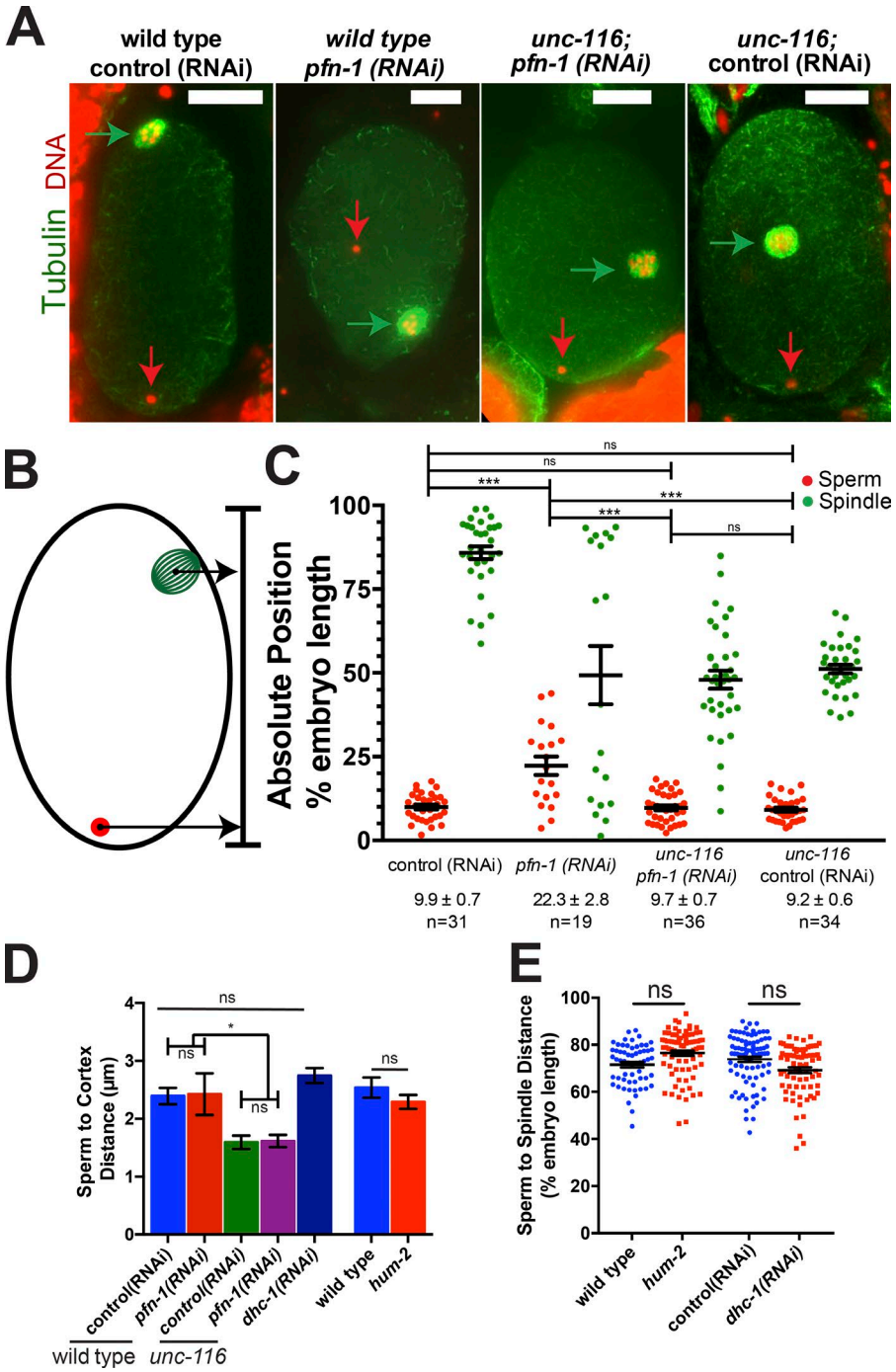

Figure 3. **Sperm DNA movement is kinesin-1 dependent.** (A) Representative images of fixed meiotic embryos. Red vertical arrows denote sperm DNA; green horizontal arrows denote the meiotic spindle. Bars, 10 µm. (B) Diagram depicting absolute position. The end of the embryo with the sperm was specified as zero. (C) Quantification of sperm and spindle positions along the long axis of the embryo in percent embryo length. (D) Quantification of the sperm-to-cortex distance in micrometers. (E) Quantification of the distance between the sperm and the meiotic spindle reported as percent embryo length. (D and E) Numbers are shown in Table S1. *, $P < 0.05$; ***, $P < 0.001$. Error bars denote standard error of the mean.

± 0.1 µm; $n = 102$; Table S1). The maximum diameter of the GFP::ubiquitin cloud was 5.3 ± 0.1 µm ($n = 67$) during metaphase I and increased throughout meiosis (Fig. 4 F). The maximum diameter of the sperm was similar in both *pfn-1(RNAi)* and control embryos (Fig. 4 G). The close proximity to the cortex and large size of the sperm contents make both cortical tethering and sieving mechanisms plausible.

A cytoplasmic actin meshwork does not restrict kinesin-1 transport in a size-dependent manner

The proposed sieving mechanism requires the existence of a deep meshwork of F-actin, which has not previously been reported during meiosis in *C. elegans*. In meiotic embryos, F-actin probes GFP::utrophin (n = 10/10), and Lifeact :mKate2 (n = 30/30) labeled a cytoplasmic meshwork (Fig. 5 A). The pattern of filaments throughout the cytoplasm resembled meshworks observed in other species (Dahlgaard et al., 2007; Schuh and Ellenberg, 2008; Mori et al., 2011). Cortical views revealed a network of asters (Fig. 5 B). Upon latrunculin A treatment of Lifeact:mKate2 meiotic embryos, the cytoplasmic meshwork and the cortical asters were abolished, but some cortical signal always remained (Fig. 5, A and B). The ratio of cortical to cytoplasm fluorescence was reduced from 2.4 ± 0.2 (n = 10) to 1.19 ± 0.2 (n = 8; $P < 0.001$). In 15/19 living embryos imaged within 3 min of

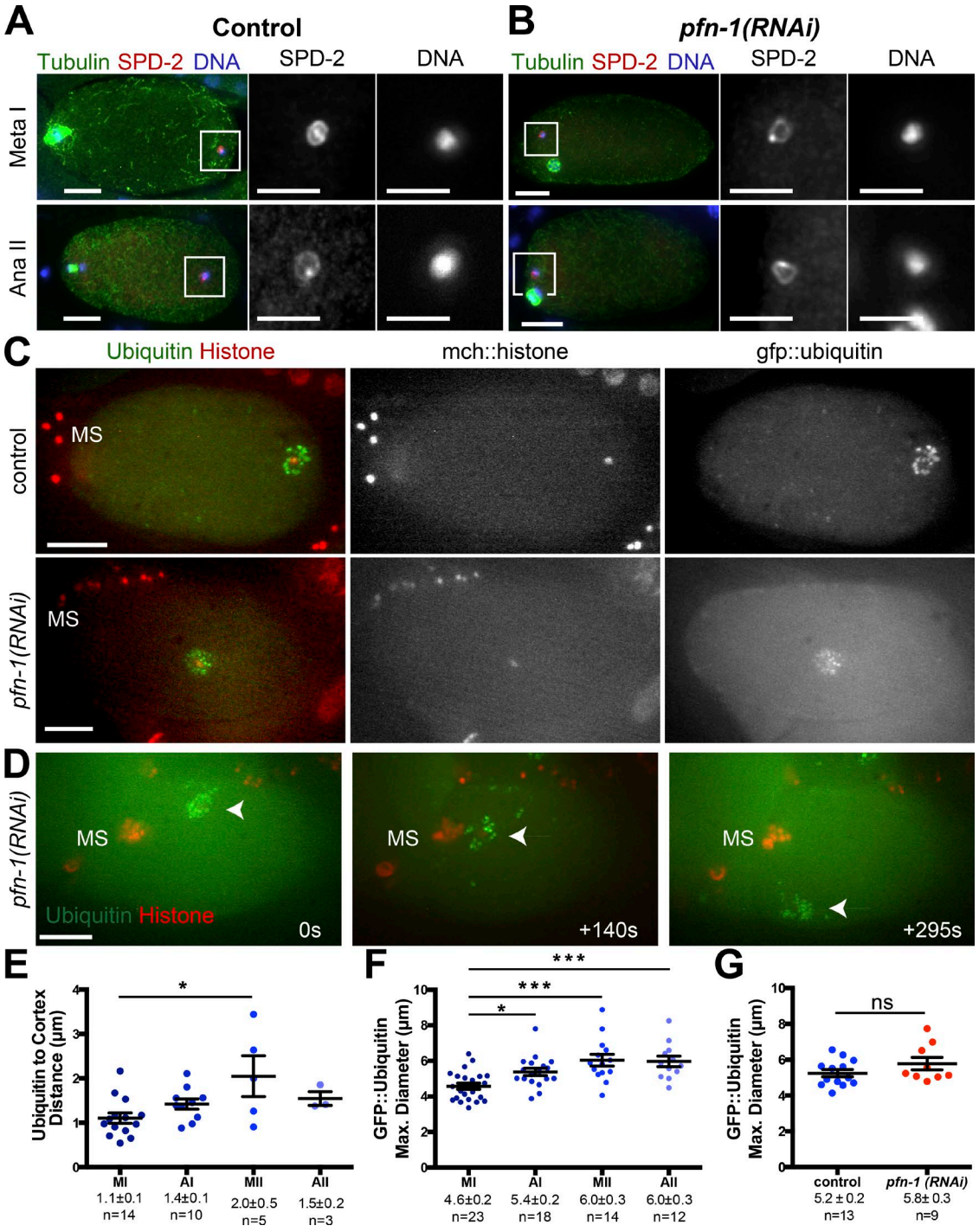

Figure 4. **The sperm centrioles and organelles move with the sperm DNA.** (A and B) Representative maximum intensity z projections of fixed control (A) or *pfn-1(RNAi)* (B) meiotic embryos stained with anti-tubulin, anti–SPD-2, and DAPI. White boxes on the merges denote the 10-µm area displayed in the inset. Ana II, anaphase II; Meta I, metaphase I. (C) Maximum intensity z projections of sperm in live meiotic embryos expressing GFP::ubiquitin and mCherry::histone (mch::histone) from a single time point after treatment with control(RNAi) or *pfn-1(RNAi)*. (D) Maximum intensity z projections of live meiotic embryos expressing GFP::ubiquitin and mCherry::histone from a time-lapse sequence. (C and D) MS indicates a meiotic spindle. Arrowheads denote the sperm. (A–D) Bars: (whole embryo) 10 µm; (inset) 5 µm. (E) Measurements of distance between ubiquitin foci and cortex by meiotic stage from fixed GFP::ubiquitin embryos stained with anti-GFP. (F) Measurements of the maximum (Max.) diameter of the ubiquitin foci surrounding the sperm in fixed GFP::ubiquitin embryos stained with anti-GFP. (E and F) AI, anaphase I; AII, anaphase II, MI, metaphase I; MII, metaphase II. (G) Measurements of the maximum diameter of the ubiquitin foci surrounding the sperm in live GFP::ubiquitin, mCherry::histone-expressing embryos treated with control(RNAi) or *pfn-1(RNAi)*, as represented in C. *, $P < 0.05$; ***, $P < 0.001$; two-tailed *t* test. Error bars denote standard error of the mean.

fertilization, actin filaments from both the cytoplasm and the cortex bent around or connected to sperm organelles (Fig. 5, C–F). To test the hypothesis that the meshwork acts as a size-dependent sieve, we depleted embryos of RAB-7 by RNAi to enlarge yolk granules by trapping them in endosomal intermediates (Grant and Hirsh, 1999; Poteryaev et al., 2007).

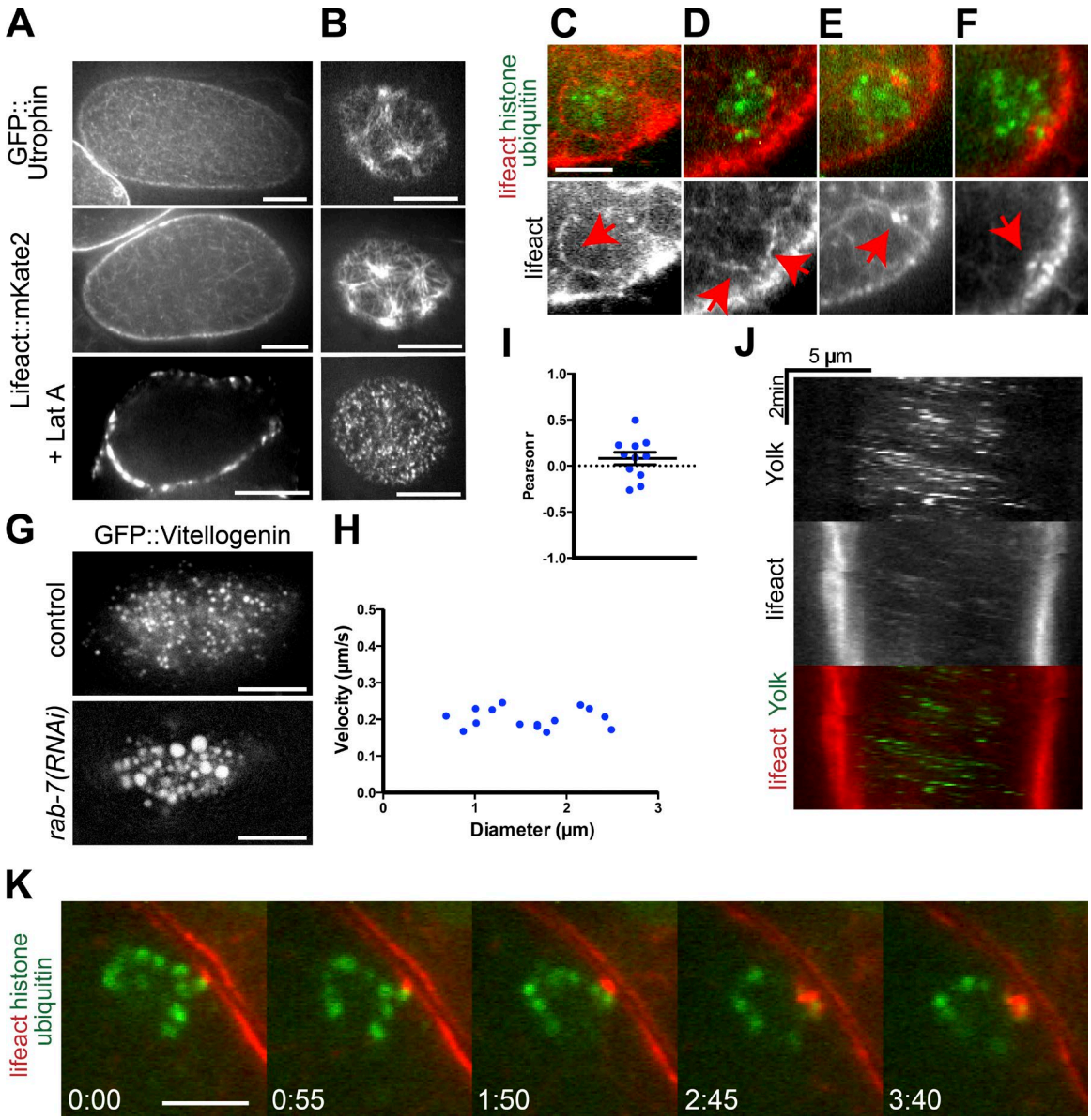

Figure 5. **Cortical F-actin, not cytoplasmic, positions the sperm.** (A and B) Mid-focal plane (A) and cortical (B) views of F-actin. Bars, 10 µm. Lat A, latrunculin A. (C–F) Single–time-point images showing various cytoplasmic and cortical F-actin structures around the sperm (arrowheads). Bar, 5 µm. (G) Single frames of subcortical yolk granules in control and *rab-7(RNAi)* meiotic embryos. Bars, 10 µm. (H) Plot of yolk granule velocity against diameter from a cluster of 15 yolk granules in a *rab-7(RNAi)* meiotic embryo. (I) Scatter plot showing the Pearson r values from 11 yolk clusters in *rab-7(RNAi)*. (J) Representative kymograph from time-lapse imaging at 5-s intervals. (K) Images from a time-lapse sequence where the sperm organelles maintain contact with the cortical actin. Bar, 5 µm.

Time-lapse imaging of GFP::yolk (see the Sperm and yolk tracking section of Materials and methods; Fig. 5 G and Videos 4–5) during metaphase I revealed that yolk granules moved with an average velocity of 0.23 ± 0.02 µm/s (n = 250; five embryos) in controls and 0.2 ± 0.03 µm/s (n = 368; five embryos) in *rab-7(RNAi)* embryos, showing that streaming occurs normally upon *rab-7(RNAi)* (Video 5). Yolk granule streaming stochastically changes in direction and varies in velocity throughout an embryo (Video 6; Kimura et al., 2017). Therefore, we compared the velocities and sizes of yolk granules within 5 µm of large (>2 µm) yolk granules (Fig. 5 H). This more direct analysis of yolk size and velocity showed that there is little correlation between yolk granule size and velocity (Fig. 5 I, Pearson's r = 0.08 ± 0.07, n = 11, sizes ranging from 0.67 to 2.58 µm). Additionally, we found that the velocity of yolk granules depends on their proximity to the center of the embryo, where the middle-most yolk granules move slower than those at the cortex (Fig. S1). These data indicate that the deep actin meshwork in wild-type embryos does not generate a size-dependent constraint on kinesin-driven motility for particles in the range of 0.8–2.5 µm. To further test the sieve hypothesis, we conducted time-lapse imaging to visualize the yolk granules as they move through the meshwork. Surprisingly, we found that deep cytoplasmic actin filaments streamed with the yolk granules (Fig. 5 J and Video 6, n = 5 embryos), making it unlikely that the deep cytoplasmic filaments could restrict movement of the sperm contents.

Cortical actin contacts the sperm contents

The cortical tethering model predicts contact between some component of the sperm contents and the cortical actin. Analysis of the cortical Lifeact::mKate2 signal using full-width half-maximum showed the cortical actin to be an average of 0.66 µm thick, whereas a gap of only 1.1 µm (Fig. 4 E) needs to be bridged between the sperm contents and the embryo cortex. Therefore, actin filaments extending at least 0.5 µm from the cortex would be required to form tethers with the sperm organelles. The time-lapse series in Fig. 5 K and Video 7 shows sperm organelles overlapping with cortical actin for nearly 4 min. This cortical sperm tethering occurs concurrently with fast cytoplasmic streaming in early meiosis just after ovulation (Video 8). These results suggest that the sperm contents are connected to the cortical actin by F-actin very early after ovulation, when kinesin-driven cytoplasmic streaming is fastest.

Elucidation of the F-actin structure that connects the sperm contents to the cortex is complicated by the fact that the Lifeact :mKate2 probe may selectively stabilize some actin structures against experimental depolymerization (Courtemanche et al., 2016). In support of this hypothesis, sperm DNA position was normal in 21/21 *pfn-1(RNAi)*–treated and 8/8 latrunculin-treated Lifeact:mKate2 meiotic embryos. 7/21 of these *pfn-1(RNAi)*–treated (Fig. S2 A) and 7/8 of these latrunculin-treated embryos (Fig. S2 B) had very bright Lifeact::mKate2 cup-like structures extending between the cortex and sperm. In a separate subset (7/21) of *pfn-1(RNAi)* embryos, Lifeact::mKate2 cages surrounded the sperm DNA (Fig. S2 C). These embryos failed to progress through meiosis. We speculate that these cup and cage structures are Lifeact-stabilized manifestations of a normally transient cortical tether and that they are made more apparent by depolymerization of other actin structures.

Our results suggest that some component of the cloud of paternal organelles surrounding the sperm DNA is bound to F-actin that is contiguous with the cortical actin. An unknown structure, likely composed of sperm-derived proteins, holds the sperm DNA, centrioles, and organelles together as a cohesive unit. The structure of this plasma membrane–less cell within a cell likely prevents incorporation of sperm DNA into the meiotic spindle, even when they are brought into close proximity after actin depletion. The cohesive nature of the sperm contents represents an unappreciated aspect of sperm and egg interactions after fertilization. SPE-11 (Browning and Strome, 1996) has long been the only example of a sperm protein required in the zygote for development in *C. elegans*. Recently, a sperm-derived PP1 phosphatase was shown to interact with maternal proteins during meiotic progression (Ataeian et al., 2016). In the future, it will be important to identify other sperm proteins required after fertilization for proper development.

Materials and methods

Worm strains

C. elegans strains were maintained as described previously (Brenner, 1974) at 20°C. N2 Bristol; WM179 *nmy-2(ne3409)* I; JCC389 *cyk-1(or596ts)* III; FM305 *sqt-1(sc103)* II; *bIs1[vit-2::GFP + rol-6(su1006)]* X; *ltIs37 [pie-1p::mCherry::his-58 + unc-119(+)]*IV; *ruls57[unc-119(+) pie-1::GFP::tubulin]*; *unc-119(ed3) III**; FM53 *unc-116(f130)* III; *unc-36(e251)*; RB801 *hum-2 (ok596)* V; LN130 *ltIs37 [pie-1p::mCherry:: his-58 + unc-119(+)]* IV; *[pie-1p::GFP::ubiquitin + unc-119(+);unc-119(ed3)]* II; LN129 *[pie-1p::GFP::ubiquitin + unc-119(+); unc-119(ed3)]* II; MG589 *mgSi3[cb-unc-119 (+) GFP::utrophin]* II; SWG001 *mex-5p::Lifeact::mKate2*; FM307 *sqt-1(sc103) II*; *bIs1[vit-2::GFP + rol-6(su1006)]* X; *ltIs37 [pie-1p::mCherry::his-58 + unc-119(+)]*IV; *unc-119(ed3)* III*; FM360 *sqt-1(sc103)* II; *bIs1[vit-2::GFP + rol-6(su1006)]* X; *mex-5p::Lifeact::mKate2*; FM347 *mjIs[mex5p::GFP::his-58::21UR-1sense::tbb-2 3′UTR]* II; *mex-5p::mkate2::Lifeact*; FM361 *[pie-1p::GFP::ubiquitin + unc-119(+)]* II; *mex-5p::mkate2::Lifeact*; *unc-119(ed3)* III*; FM418 *[pie-1p::GFP::ubiquitin + unc-119(+)]* II; *mjIs[mex5p:: GFP::his-58::21UR-1sense::tbb-2 3′UTR]* II; and *mex-5p::mkate2::Lifeact; unc-119(ed3)* III* were used. An asterisk indicates that these genotypes show *[unc-119(ed3)*]*, as this mutation was present in the parental strains but has not been directly sequenced in these strains to determine whether the *unc-119* gene is mutated.

In utero microscopy

Adult hermaphrodites were anesthetized with tricaine/tetramisole in PBS and immobilized between a coverslip and agarose pad on a slide. Imaging for Figs. 1, 2, 3, 4A, and 5G was done using MicroManager with a microscope (IX81; Olympus) equipped with an oil objective (60× PlanApo 1.42), a disk-scanning unit (Olympus), and a camera (ORCA Flash 4.0 CMOS; Hamamatsu Photonics). Imaging for Figs. 4 (C and D) and 5 (A–F, J, and K) were captured using Velocity on a Cetus Ultraview Spinning Disk Confocal microscope (PerkinElmer) equipped with a camera (Orca R2 CCD; Hamamatsu Photonics) and an oil objective (100× 1.35; Olympus). Fig. 2 (A–C) was deconvolved using Huygens Professional X11 (SVI). Fig. 5 G, Fig. S1, and Videos 1–5 were processed using ImageJ (National Institutes of Health) Rolling Ball Background Subtraction.

Immunofluorescence

C. elegans meiotic embryos were extruded from hermaphrodites in 0.8× egg buffer by gently squishing worms between coverslip and slide, flash frozen in liquid N_2, permeabilized by removing the coverslip, and then fixed in cold methanol before staining with antibodies and DAPI. Primary antibodies used in this work were mouse monoclonal anti-tubulin (DM1α; Sigma-Aldrich), anti–SPD-2 (provided by K. Oegema, University of California, San Diego, La Jolla, CA), and anti-GFP (Novus). Secondary antibodies used were Alexa Fluor 594 anti–mouse, Alexa Fluor 594 anti–rabbit, and Alexa Fluor 488 anti–mouse (Molecular Probes). Complete z stacks were captured for each meiotic embryo with an inverted microscope (IX81) equipped with an oil objective (60× PlanApo 1.42), a disk-scanning unit (Olympus), and a camera (ORCA Flash 4.0 CMOS).

RNA interference and drug treatments

All of the RNAi experiments were performed by feeding bacteria (HT115) induced to express double-stranded RNA to each gene. Clones were taken from the Ahringer RNAi library: II-8513(*RAB-7*), II-7B17(*ECT-2*), I-6F19(*PFN-1*), III-3P11(*CYK-1*), and I-1P04(*DHC-1*) (Kamath et al., 2003). L4 hermaphrodites were transferred to RNAi plates and allowed to feed on the RNAi bacterial lawn for 24–48 h. For fixed experiments, worms were incubated in 0.8× egg buffer with 100 µM latrunculin A (no. 428021; Millipore) for 1 h or 500 µM SMIFH2 (no. 344092; Millipore) for 30 min. For live experiments, drugs were used at the same concentration and duration while the worms were being anesthetized. Embryos considered to have a strong depletion of F-actin included metaphase I and anaphase I embryos adjacent to an older mitotic embryo with no polar bodies, metaphase II embryos that had 12 chromosomes and no polar body (Fig. 1 A), and anaphase II embryos with no polar body and very large spindles.

Sperm position and size measurements

Distances were measured using ImageJ. For sperm DNA–to-cortex distance, we measured from the edge of the sperm DNA to the embryo edge as seen by the tubulin staining. For sperm organelle-to-cortex distance, we measured from the edge of the anti-GFP signal in GFP::ubiquitin-expressing embryos to the embryo edge as seen by the tubulin staining. Embryos where the sperm was clearly closer in the z axis were not included. For sperm-to-spindle distance, we measured the edge of the sperm DNA to the edge of the tubulin staining of the spindle during metaphase or the edge of the chromosomes during anaphase. Distance between the spindle and the sperm DNA was scored as percent embryo length because *pfn-1(RNAi)* embryos were variable in absolute length. For sperm-to-spindle distance measurements, embryos with lateral or mispositioned spindles were not quantified (we analyzed the 84% of control and 79% of *pfn-1[RNAi]* meiotic embryos that had the meiotic spindle positioned at the future anterior end of the oval embryo). The change in z axis was included in these distances. Distances were normalized against embryo length. Absolute position in Fig. 3 C was scored in a manner where the sperm was always closer to zero percent embryo length. The center of the spindle and sperm yielded the position along the percent embryo length. The maximum diameter of the sperm was measured in a single plane using the edges of the GFP::ubiquitin signal in live embryos and the edges of the anti-GFP signal in GFP::ubiquitin-fixed embryos.

Sperm and yolk tracking

For sperm imaging, after identifying early meiosis I embryos, the focal plane was adjusted to find the sperm manually. Then, acquisition began using 2.5-, 5-, or 10-s intervals, and the sperm was manually tracked during time-lapse imaging, manually adjusting the stage (z axis) to keep the sperm DNA in focus. For yolk granule imaging, after identifying early meiotic embryos, the focal plane was adjusted to a near cortical view before acquisition at 5-s intervals. Yolk granules were imaged in a subcortical view, as they stayed in focus for several frames and were easier to distinguish because of reduced out-of-focus light typical of a mid-plane view. Then, trajectories were generated using the ImageJ plugin Manual Tracking. A minimum of 50 yolk granules was tracked per embryo. For yolk cluster analysis in *rab-7(RNAi)*, the velocities of a minimum of 10 yolk granules were plotted against their diameter and analyzed using Pearson's correlation. Yolk granules had to be within 5 µm of a large yolk granule with a diameter >2 µm.

MSD and maximum displacement

The x-y positions from the Manual Tracking plugin in ImageJ and the change in stage position for the change in z position were used for MSD analysis. 3D MSD with internal averaging was calculated for the duration of the trajectory using Matlab. Individual MSDs were combined to give an averaged 3D MSD and plotted up to one fourth of the shortest trajectory (Saxton, 1997) and fit to an exponential line to give α (Fig. 2 F). Individual time-lapse sequences were plotted up to one fourth of the total duration (Fig. 2 H). Only trajectories with an acquisition interval of 5 s were used for this analysis. For maximum displacement, the maximum x-y displacement in a 30-s time frame was used and compared between images acquired at 2.5-, 5-, and 10-s intervals.

Full-width half-maximum

A macro in Fiji was used to determine the full-width half-maximum from intensity profiles and Gaussian fitting (adapted from John Lim, IMB). Measurements were taken in mid-focal planes, and 10 measurements were taken per embryo. Measurements had to have a Gaussian fit of $R^2 > 0.9$.

Online supplemental material

Fig. S1 shows Yolk granule velocity depends on distance from the center of the embryo. Fig. S2 shows partial F-actin depletion reveals Lifeact::mKate2-stabilized structures near the sperm. Table S1 shows sperm distances related to Figs. 1 and 3. Video 1 shows sperm DNA is restricted to a confined space. Video 2 shows sperm DNA moves after *pfn-1(RNAi)* treatment. Video 3 shows sperm DNA moves close to the cortex after *pfn-1(RNAi)* treatment. Video 4 shows yolk granule transport in a control embryo. Video 5 shows yolk granule transport after *rab-7(RNAi)* treatment. Video 6 shows actin filaments and yolk granules stream together. Video 7 shows sperm organelles contact cortical F-actin. Video 8 shows F-actin and yolk granule dynamics throughout all stages of meiosis.

Acknowledgments

We thank Ingrid Brust-Mascher and Taryn Gillies for assistance with MSD analysis. We thank Brian Cook for his initial observations that led to this project and Karen McNally for critical reading of the manuscript. We thank Lynn Boyd and the Caenorhabditis Genetics Center, which is funded by the National Institutes of Health Office of Research Infrastructure Programs (grant P40 OD010440), for strains.

This work was supported by National Institute of General Medical Sciences grant 1R01GM-079421 and U.S. Department of Agriculture National Institute of Food and Agriculture Hatch project 1009162 (to F.J. McNally).

The authors declare no competing financial interests.

Author contributions: M.T. Panzica: conceptualization, formal analysis, investigation, methodology, writing, review, and editing; H.C. Marin: formal analysis, investigation, review, and editing; A.-C. Reymann: investigation and resources; F.J. McNally: conceptualization, funding acquisition, writing, review, and editing.

Submitted: 3 February 2017
Revised: 17 April 2017
Accepted: 18 May 2017

References

Al Rawi, S., S. Louvet-Vallée, A. Djeddi, M. Sachse, E. Culetto, C. Hajjar, L. Boyd, R. Legouis, and V. Galy. 2011. Postfertilization autophagy of sperm organelles prevents paternal mitochondrial DNA transmission. *Science.* 334:1144–1147. http://dx.doi.org/10.1126/science.1211878

Ataeian, M., J. Tegha-Dunghu, D.G. Curtis, E.M. Sykes, A. Nozohourmehrabad, M. Bajaj, K. Cheung, and M. Srayko. 2016. Maternal MEMI promotes female meiosis II in response to fertilization in *Caenorhabditis elegans*. *Genetics.* 204:1461–1477. http://dx.doi.org/10.1534/genetics.116.192997

Baker, J.P., and M.A. Titus. 1997. A family of unconventional myosins from the nematode *Caenorhabditis elegans*. *J. Mol. Biol.* 272:523–535. http://dx.doi.org/10.1006/jmbi.1997.1232

Brenner, S. 1974. The genetics of *Caenorhabditis elegans*. *Genetics.* 77:71–94.

Browning, H., and S. Strome. 1996. A sperm-supplied factor required for embryogenesis in *C. elegans*. *Development.* 122:391–404.

Chang, F., D. Drubin, and P. Nurse. 1997. cdc12p, a protein required for cytokinesis in fission yeast, is a component of the cell division ring and interacts with profilin. *J. Cell Biol.* 137:169–182. http://dx.doi.org/10.1083/jcb.137.1.169

Courtemanche, N., T.D. Pollard, and Q. Chen. 2016. Avoiding artefacts when counting polymerized actin in live cells with LifeAct fused to fluorescent proteins. *Nat. Cell Biol.* 18:676–683. http://dx.doi.org/10.1038/ncb3351

Dahlgaard, K., A.A. Raposo, T. Niccoli, and D. St Johnston. 2007. Capu and Spire assemble a cytoplasmic actin mesh that maintains microtubule organization in the *Drosophila* oocyte. *Dev. Cell.* 13:539–553. http://dx.doi.org/10.1016/j.devcel.2007.09.003

Deguchi, R., H. Shirakawa, S. Oda, T. Mohri, and S. Miyazaki. 2000. Spatiotemporal analysis of Ca^{2+} waves in relation to the sperm entry site

and animal–vegetal axis during Ca^{2+} oscillations in fertilized mouse eggs. *Dev. Biol.* 218:299–313. http://dx.doi.org/10.1006/dbio.1999.9573

Evangelista, M., K. Blundell, M.S. Longtine, C.J. Chow, N. Adames, J.R. Pringle, M. Peter, and C. Boone. 1997. Bni1p, a yeast formin linking cdc42p and the actin cytoskeleton during polarized morphogenesis. *Science.* 276:118–122. http://dx.doi.org/10.1126/science.276.5309.118

Goldstein, B., and S.N. Hird. 1996. Specification of the anteroposterior axis in *Caenorhabditis elegans. Development.* 122:1467–1474.

Gould, M.C., and J.L. Stephano. 1999. MAP kinase, meiosis, and sperm centrosome suppression in *Urechis caupo*. *Dev. Biol.* 216:348–358. http://dx.doi.org/10.1006/dbio.1999.9468

Grant, B., and D. Hirsh. 1999. Receptor-mediated endocytosis in the *Caenorhabditis elegans* oocyte. *Mol. Biol. Cell.* 10:4311–4326. http://dx.doi.org/10.1091/mbc.10.12.4311

Hajjar, C., K.M. Sampuda, and L. Boyd. 2014. Dual roles for ubiquitination in the processing of sperm organelles after fertilization. *BMC Dev. Biol.* 14:6. http://dx.doi.org/10.1186/1471-213X-14-6

Kamath, R.S., A.G. Fraser, Y. Dong, G. Poulin, R. Durbin, M. Gotta, A. Kanapin, N. Le Bot, S. Moreno, M. Sohrmann, et al. 2003. Systematic functional analysis of the *Caenorhabditis elegans* genome using RNAi. *Nature.* 421:231–237. http://dx.doi.org/10.1038/nature01278

Kapitein, L.C., P. van Bergeijk, J. Lipka, N. Keijzer, P.S. Wulf, E.A. Katrukha, A. Akhmanova, and C.C. Hoogenraad. 2013. Myosin-V opposes microtubule-based cargo transport and drives directional motility on cortical actin. *Curr. Biol.* 23:828–834. http://dx.doi.org/10.1016/j.cub.2013.03.068

Kimura, K., A. Mamane, T. Sasaki, K. Sato, J. Takagi, R. Niwayama, L. Hufnagel, Y. Shimamoto, J.F. Joanny, S. Uchida, and A. Kimura. 2017. Endoplasmic-reticulum-mediated microtubule alignment governs cytoplasmic streaming. *Nat. Cell Biol.* 19:399–406. http://dx.doi.org/10.1038/ncb3490

McCarter, J., B. Bartlett, T. Dang, and T. Schedl. 1999. On the control of oocyte meiotic maturation and ovulation in *Caenorhabditis elegans*. *Dev. Biol.* 205:111–128. http://dx.doi.org/10.1006/dbio.1998.9109

McNally, K.L., J.L. Martin, M. Ellefson, and F.J. McNally. 2010. Kinesin-dependent transport results in polarized migration of the nucleus in oocytes and inward movement of yolk granules in meiotic embryos. *Dev. Biol.* 339:126–140. http://dx.doi.org/10.1016/j.ydbio.2009.12.021

McNally, K.L., A.S. Fabritius, M.L. Ellefson, J.R. Flynn, J.A. Milan, and F.J. McNally. 2012. Kinesin-1 prevents capture of the oocyte meiotic spindle by the sperm aster. *Dev. Cell.* 22:788–798. http://dx.doi.org/10.1016/j.devcel.2012.01.010

Mi-Mi, L., S. Votra, K. Kemphues, A. Bretscher, and D. Pruyne. 2012. Z-line formins promote contractile lattice growth and maintenance in striated muscles of *C. elegans*. *J. Cell Biol.* 198:87–102. http://dx.doi.org/10.1083/jcb.201202053

Mori, M., N. Monnier, N. Daigle, M. Bathe, J. Ellenberg, and P. Lénárt. 2011. Intracellular transport by an anchored homogeneously contracting F-actin meshwork. *Curr. Biol.* 21:606–611. http://dx.doi.org/10.1016/j.cub.2011.03.002

Motegi, F., and A. Sugimoto. 2006a. Function of microtubules at the onset of cytokinesis. *Tanpakushitsu Kakusan Koso.* 51:1590–1595.

Motegi, F., and A. Sugimoto. 2006b. Sequential functioning of the ECT-2 RhoGEF, RHO-1 and CDC-42 establishes cell polarity in *Caenorhabditis elegans* embryos. *Nat. Cell Biol.* 8:978–985. http://dx.doi.org/10.1038/ncb1459

Pelletier, L., N. Ozlü, E. Hannak, C. Cowan, B. Habermann, M. Ruer, T. Müller-Reichert, and A.A. Hyman. 2004. The *Caenorhabditis elegans* centrosomal protein SPD-2 is required for both pericentriolar material recruitment and centriole duplication. *Curr. Biol.* 14:863–873. http://dx.doi.org/10.1016/j.cub.2004.04.012

Poteryaev, D., H. Fares, B. Bowerman, and A. Spang. 2007. *Caenorhabditis elegans* SAND-1 is essential for RAB-7 function in endosomal traffic. *EMBO J.* 26:301–312. http://dx.doi.org/10.1038/sj.emboj.7601498

Rizvi, S.A., E.M. Neidt, J. Cui, Z. Feiger, C.T. Skau, M.L. Gardel, S.A. Kozmin, and D.R. Kovar. 2009. Identification and characterization of a small molecule inhibitor of formin-mediated actin assembly. *Chem. Biol.* 16:1158–1168. http://dx.doi.org/10.1016/j.chembiol.2009.10.006

Runge, K.E., J.E. Evans, Z.Y. He, S. Gupta, K.L. McDonald, H. Stahlberg, P. Primakoff, and D.G. Myles. 2007. Oocyte CD9 is enriched on the microvillar membrane and required for normal microvillar shape and distribution. *Dev. Biol.* 304:317–325. http://dx.doi.org/10.1016/j.ydbio.2006.12.041

Sagot, I., A.A. Rodal, J. Moseley, B.L. Goode, and D. Pellman. 2002. An actin nucleation mechanism mediated by Bni1 and profilin. *Nat. Cell Biol.* 4:626–631.

Saxton, M.J. 1997. Single-particle tracking: the distribution of diffusion coefficients. *Biophys. J.* 72:1744–1753. http://dx.doi.org/10.1016/S0006-3495(97)78820-9

Schuh, M., and J. Ellenberg. 2008. A new model for asymmetric spindle positioning in mouse oocytes. *Curr. Biol.* 18:1986–1992. http://dx.doi.org/10.1016/j.cub.2008.11.022

Serbus, L.R., B.J. Cha, W.E. Theurkauf, and W.M. Saxton. 2005. Dynein and the actin cytoskeleton control kinesin-driven cytoplasmic streaming in *Drosophila* oocytes. *Development.* 132:3743–3752. http://dx.doi.org/10.1242/dev.01956

Severson, A.F., D.L. Baillie, and B. Bowerman. 2002. A Formin Homology protein and a profilin are required for cytokinesis and Arp2/3-independent assembly of cortical microfilaments in *C. elegans*. *Curr. Biol.* 12:2066–2075. http://dx.doi.org/10.1016/S0960-9822(02)01355-6

Shaye, D.D., and I. Greenwald. 2016. A network of conserved formins, regulated by the guanine exchange factor EXC-5 and the GTPase CDC-42, modulates tubulogenesis in vivo. *Development.* 143:4173–4181. http://dx.doi.org/10.1242/dev.141861

Stephano, J.L., and M.C. Gould. 2000. MAP kinase, a universal suppressor of sperm centrosomes during meiosis? *Dev. Biol.* 222:420–428. http://dx.doi.org/10.1006/dbio.2000.9726

Swan, K.A., A.F. Severson, J.C. Carter, P.R. Martin, H. Schnabel, R. Schnabel, and B. Bowerman. 1998. cyk-1: a *C. elegans* FH gene required for a late step in embryonic cytokinesis. *J. Cell Sci.* 111:2017–2027.

Takayama, J., and S. Onami. 2016. The sperm TRP-3 channel mediates the onset of a Ca^{2+} wave in the fertilized *C. elegans* oocyte. *Cell Reports.* 15:625–637. http://dx.doi.org/10.1016/j.celrep.2016.03.040

Verlhac, M.H., C. Lefebvre, P. Guillaud, P. Rassinier, and B. Maro. 2000. Asymmetric division in mouse oocytes: with or without Mos. *Curr. Biol.* 10:1303–1306. http://dx.doi.org/10.1016/S0960-9822(00)00753-3

Ward, S., Y. Argon, and G.A. Nelson. 1981. Sperm morphogenesis in wild-type and fertilization-defective mutants of *Caenorhabditis elegans*. *J. Cell Biol.* 91:26–44. http://dx.doi.org/10.1083/jcb.91.1.26

Watanabe, N., P. Madaule, T. Reid, T. Ishizaki, G. Watanabe, A. Kakizuka, Y. Saito, K. Nakao, B.M. Jockusch, and S. Narumiya. 1997. p140mDia, a mammalian homolog of *Drosophila* diaphanous, is a target protein for Rho small GTPase and is a ligand for profilin. *EMBO J.* 16:3044–3056. http://dx.doi.org/10.1093/emboj/16.11.3044

Yang, H.Y., K. McNally, and F.J. McNally. 2003. MEI-1/katanin is required for translocation of the meiosis I spindle to the oocyte cortex in *C. elegans*. *Dev. Biol.* 260:245–259. http://dx.doi.org/10.1016/S0012-1606(03)00216-1

Yi, K., J.R. Unruh, M. Deng, B.D. Slaughter, B. Rubinstein, and R. Li. 2011. Dynamic maintenance of asymmetric meiotic spindle position through Arp2/3-complex-driven cytoplasmic streaming in mouse oocytes. *Nat. Cell Biol.* 13:1252–1258. http://dx.doi.org/10.1038/ncb2320

Yoder, J.H., and M. Han. 2001. Cytoplasmic dynein light intermediate chain is required for discrete aspects of mitosis in *Caenorhabditis elegans*. *Mol. Biol. Cell.* 12:2921–2933. http://dx.doi.org/10.1091/mbc.12.10.2921